Kamath, Arun; Bihs, Hans; Arntsen, Øivind Asgeir

A CFD based 3D Numerical Wave Tank to Investigate Wave Interaction with Rectangular Cylinders

ICHE 2014, Hamburg - Lehfeldt & Kopmann (eds) - © 2014 Bundesanstalt für Wasserbau ISBN 978-3-939230-32-8

A CFD based 3D Numerical Wave Tank to Investigate Wave Interaction with Rectangular Cylinders

A. Kamath & H. Bihs & Ø.A. Arntsen
Department of Civil and Transport Engineering
Norwegian University of Science and Technology, Trondheim, Norway

ABSTRACT: Cylinders with rectangular cross-sections find application in the design of offshore structures due to the ease in manufacture and transport in comparison to circular elements. Rectangular sections can also be seen in the design of tension leg platforms and floating production units. The fluid flow problem is changed due to the introduction of asymmetry and the aspect ratio of a rectangular cross-section which influences the flow regime. So, gaining more knowledge about the hydrodynamics of the flow around a rectangular cylinder and the wave forces acting on the cylinder is of practical interest. This paper investigates the interaction of regular waves with a truncated rectangular cylinder using a Computational Fluid Dynamics (CFD) model. The influence of the aspect ratio of the cylinder with respect to the incident wavelength is investigated and the force experienced by the cylinder under different aspect ratios is calculated. The numerical results are compared with experimental data.

Keywords: CFD, Rectangular cylinders, Wave force, Numerical wave tank, REEF3D

1 INTRODUCTION

Offshore constructions are generally composed of cylindrical elements of circular cross section. A lot of research has been carried out to understand wave interaction with circular cylindrical structures for example by Morison et al. (1950), Keulegan and Carpenter (1958), Sarpkaya (1976) and Mo et al. (2007). There are empirical and analytical formulae that can be used to calculate wave forces on circular cylinders such as the Morison formula (Morison et al., 1954) and the MacCamy-Fuchs diffraction theory (MacCamy and Fuchs, 1954) for different types of flow regimes around circular cylinders. On the other hand, not many studies have been carried out to investigate the wave interaction with cylinders of rectangular cross-sections. Due to the presence of sharp corners in a rectangular cross-section, the force coefficients are different for these cylinders compared to circular cylinders (Bearman et al., 1979) and the standard force coefficients used in the Morison formula are not applicable. An investigation into flow around rectangular cylinders and the wave forces acting on them can provide insight into the hydrodynamics around them.

Computational Fluid Dynamics (CFD) uses the Navier-Stokes equations to solve the fluid flow problem. This accounts for most of the flow physics and provides detailed information regarding the flow. Flow parameters such as fluid particle velocities, free surface elevation and flow patterns around the cylinders can be studied in a detailed manner. The wave forces acting on the cylinders can be calculated and the variation of the force on the cylinder for various configurations of a rectangular cylinder can be studied.

In this study, an open source CFD model REEF3D, is employed to study wave interaction with truncated rectangular cylinders. A cylinder with a rectangular cross-section is placed in a 3D numerical wave tank and exposed to regular periodic waves. Wave interaction with five different cylinder aspect ratios are simulated and the wave forces acting on the cylinder in each case is studied. The wave elevation contours around the cylinders in each of the cases are also studied to obtain a better understanding of the flow field.

2 NUMERICAL MODEL

2.1 *Governing Equations*

The numerical model solves the fluid flow problem using the incompressible Reynolds-averaged Navier-Stokes (RANS) equations along with the continuity equation:

$$\frac{\partial U_i}{\partial x_i} = 0 \tag{1}$$

$$\frac{\partial U_i}{\partial t} + U_j \frac{\partial U_i}{\partial x_j} = -\frac{1}{\rho}\frac{\partial P}{\partial x_i} + \frac{\partial}{\partial x_j}\left[\left(v + v_t\right)\left(\frac{\partial U_i}{\partial x_j} + \frac{\partial U_j}{\partial x_i}\right)\right] + g_i \tag{2}$$

where U is the time averaged velocity, ρ is the density of water, P is the pressure, v is the kinematic viscosity, v_t is the eddy viscosity, t is time and g is the acceleration due to gravity.

Turbulence modeling is carried out using the two equation $k - \omega$ turbulence model (Wilcox, 1994). The highly strained flow due to the waves results in an unphysical overproduction of turbulence. This is reduced using the eddy viscosity limiters proposed by Durbin (2009). The free surface is a natural boundary where the eddy viscosity is damped, but the k-ω model does not account for this. This results in overproduction of turbulence at the interface between water and air in a two-phase model. This is reduced using limiters on the turbulent source terms as shown by Egorov (2004) at the free surface using the Dirac delta function.

2.2 *Free Surface*

The free surface is obtained using the level set method (Osher and Sethian, 1988). In this method, the interface between the two fluids is represented by the zero level set of the function. For the rest of the domain, the level set function (ϕ) provides the least distance from the interface and the different fluids are identified by the sign of the level set function. The level set function loses its signed-distance property on convection and it is reinitialised after every iteration using a partial differential equation based method shown by Peng et al. (1999) to restore the signed-distance property of the function.

2.3 *Discretisation Schemes*

A conservative fifth-order Weighted Essentially Non-Oscillatory (WENO) scheme (Jiang and Shu, 1996) is used to discretise the convective terms of the RANS equations. The Hamilton-Jacobi formulation of the WENO scheme (Jiang and Peng, 2000) is used to discretise the turbulent kinetic energy (k), the specific turbulent dissipation (ω) and the level set function (ϕ). The explicit third-order total variation diminishing Runge-Kutta scheme is used for time advancement of the level set function and the reinitialisation equation. Numerical stability of the simulation is ensured through an adaptive time stepping scheme satisfying the CFL criterion based on the maximum velocity in the domain. A first-order implicit scheme is used for the time advancement of the turbulent kinetic energy and the specific turbulent dissipation rate. These terms are mainly source term driven with a low influence of the convective terms and the large source terms can result in very small time steps due to the turbulence model. With an implicit treatment of these terms, the time steps are based on the maximum velocity in the domain. The diffusion terms of the velocity are also treated with a first-order implicit scheme to base the time steps on the maximum velocity in the domain.

2.4 *Numerical Wave Tank*

The numerical wave tank uses the relaxation method (Larsen and Dancy, 1983) for wave generation and absorption. In this method, a portion of the wave tank is reserved as relaxation zones for wave generation and absorption. Relaxation functions are used in these zones to moderate the numerical values for the velocities and the free surface. In the wave generation zone, the relaxation function prescribes the values for velocities and free surface from the wave theory used for the simulation and generates waves which are then released into the working zone of the tank. The objects to be studied are placed in the working zone of the tank. The wave absorption relaxation zone is located at the end of the working zone of the wave

tank. The relaxation function in this zone reduces the computational values of velocities from the wave tank to zero, returns the free surface to the still water level and the pressure to its hydrostatic value. This method requires an explicit allocation of zones in the tank for wave generation and absorption. This increases the computational cost of the numerical simulations but provides an accurate representation of the waves in the numerical wave tank.

3 EXPERIMENTAL AND NUMERICAL SETUP

The data from the experiments carried out by Vengatesan et al. (2000) is used for the comparison of the numerical results. The experiments were carried out in the towing tank of the Hydrodynamic Laboratory at the Department of Naval Architecture and Ocean Engineering at the University of Glasgow. The tank is 4.6m wide, 2.7m deep and 77m long, equipped with a paddle/flap wavemaker. A rectangular cylinder 2m high with a cross-section of 0.4m × 0.2m in a water depth d = 2.2m with a depth of immersion of 1.45m is exposed to waves of different wave periods and wave heights. The effect of the aspect ratio of the cylinder on the wave forces experienced by it is studied by carrying out experiments with the broad side and the narrow side of the cylinder facing the waves. The aspect ratio (AR) is defined as the ratio between the side normal to wave propagation to the side along the direction of wave propagation. The force coefficients C_m and C_d to be used in the Morison formula for calculating inline wave forces on rectangular cylinders are determined in the experiments.

At first, a numerical simulation is carried out with a rectangular cylinder with an aspect ratio, AR = 2/1 exposed to incident waves of wavelength λ = 3.84m and wave height H = 0.064m and the results are compared to the forces obtained using the Morison formula with the force coefficients determined in the experiments by Vengatesan et al. (2000) to obtain confidence in the numerical results. In order to study the wave interaction with rectangular cylinders of different aspect ratios, the width of the cylinder in the direction of wave propagation, l is varied. The details of the cylinder configurations used in the simulations are given in Table 1.

Table 1. Overview of simulations carried out in the study

Case	Aspect ratio (AR)	b(m)	l(m)
1	2/1	0.4	0.2
2	1/4	0.4	1.6
3	1/2	0.4	0.8
4	1/1	0.4	0.4
5	4/1	0.4	0.1

The working zone of the numerical wave tank is kept about three wavelengths long with one wavelength long wave generation relaxation zone and a two wavelength long wave absorption zone. The numerical wave tank is 24m long, 4.6m wide and 4.4m high. A grid size of dx = 0.05m is used for the simulations, which results in a numerical wave tank with 3.89 million cells illustrated in Figure 1.

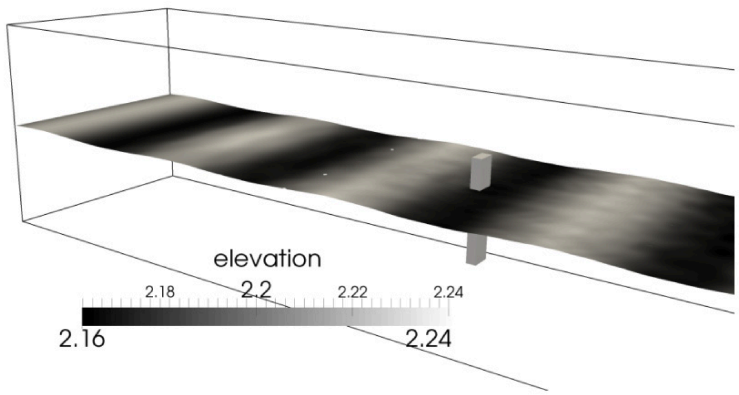

Figure 1. Numerical wave tank setup for the simuations.

4 RESULTS

The numerical results for the first case with an aspect ratio of 2/1 is compared to the force expected using the Morison formula with the force coefficients determined through experiments in Figure 2. The Morison force coefficients determined in the experiments for this case are C_m = 3.59 and C_d = 9.35 (Vengatesan et al., 2000). The numerically determined forces show a good agreement to the values determined by the Morison formula. A grid convergence study for the wave forces is carried out by simulating the setup with grid sizes dx = 0.1m and dx = 0.2m and compared to the numerical result calculated with a grid size of dx = 0.05m and the force obtained using the Morison formula. It is seen in Figure 3 that the wave forces are underestimated at lower grid resolutions and the calculated force shows a better agreement with the value obtained using the Morison formula at a grid size of dx = 0.05m. This grid size is then used for the rest of the numerical simulations in the study.

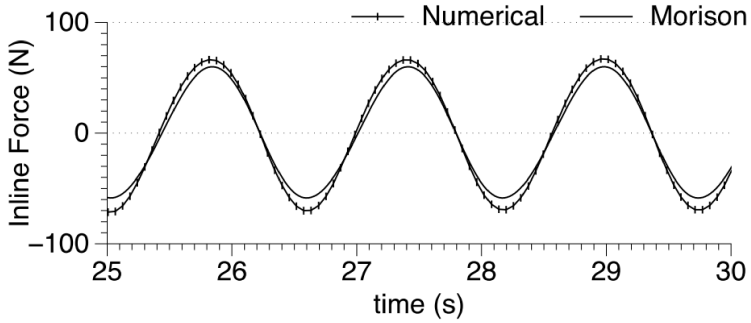

Figure 2. Wave force on cylinder with AR = 2/1.

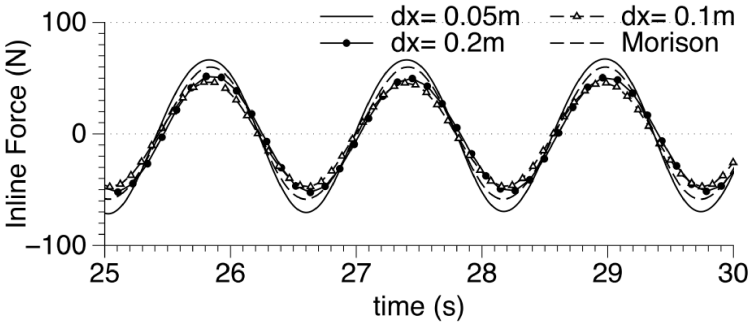

Figure 3. Grid convergence study for wave force on the cylinder with AR = 2/1.

The numerical model is then used to study the variation of the inline wave forces with the aspect ratio of the cylinder. The numerical results for wave forces for cylinder aspect ratios AR of 1/4, 1/2, 1/1 and 4/1 exposed to an incident wavelength of λ = 3.84m and wave height H = 0.064m are presented in Figure 4.

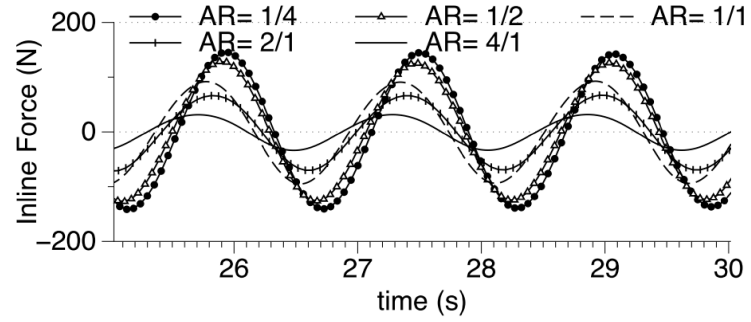

Figure 4. Wave forces on the cylinder for different aspect ratios.

It is observed that the inline wave forces on the cylinder increase with decreasing aspect ratio and they are reduced on increasing the aspect ratio. Thus, for a given breadth of the cross-section b normal to the direction of wave propagation, an increase in the width of the cross-section l along the direction of wave propagation increases the wave forces acting on the cylinder. The change in the magnitude of the force for an increase of the aspect ratio from 1/4 to 1/2 not too large, but a large change in the magnitude of the force is seen on further increase of the aspect ratio from 1/2 to 1/1, 2/1 and 4/1. The phase of the forces acting on the cylinder is also seen to vary with the aspect ratio. The calculated force signal for ahigher as-

pect ratio leads the calculated force signal for cylinders with a lower aspect ratio. This is because the width of the cylinder in the direction of wave propagation has a direct influence on the resulting inline wave forces on the cylinder. The cylinders with a longer cross-sectional width (l) are influenced by the net pressure difference between its front and back faces earlier than the cylinders whose cross-sectional widths are smaller, resulting in the phase difference seen in Figure 4.

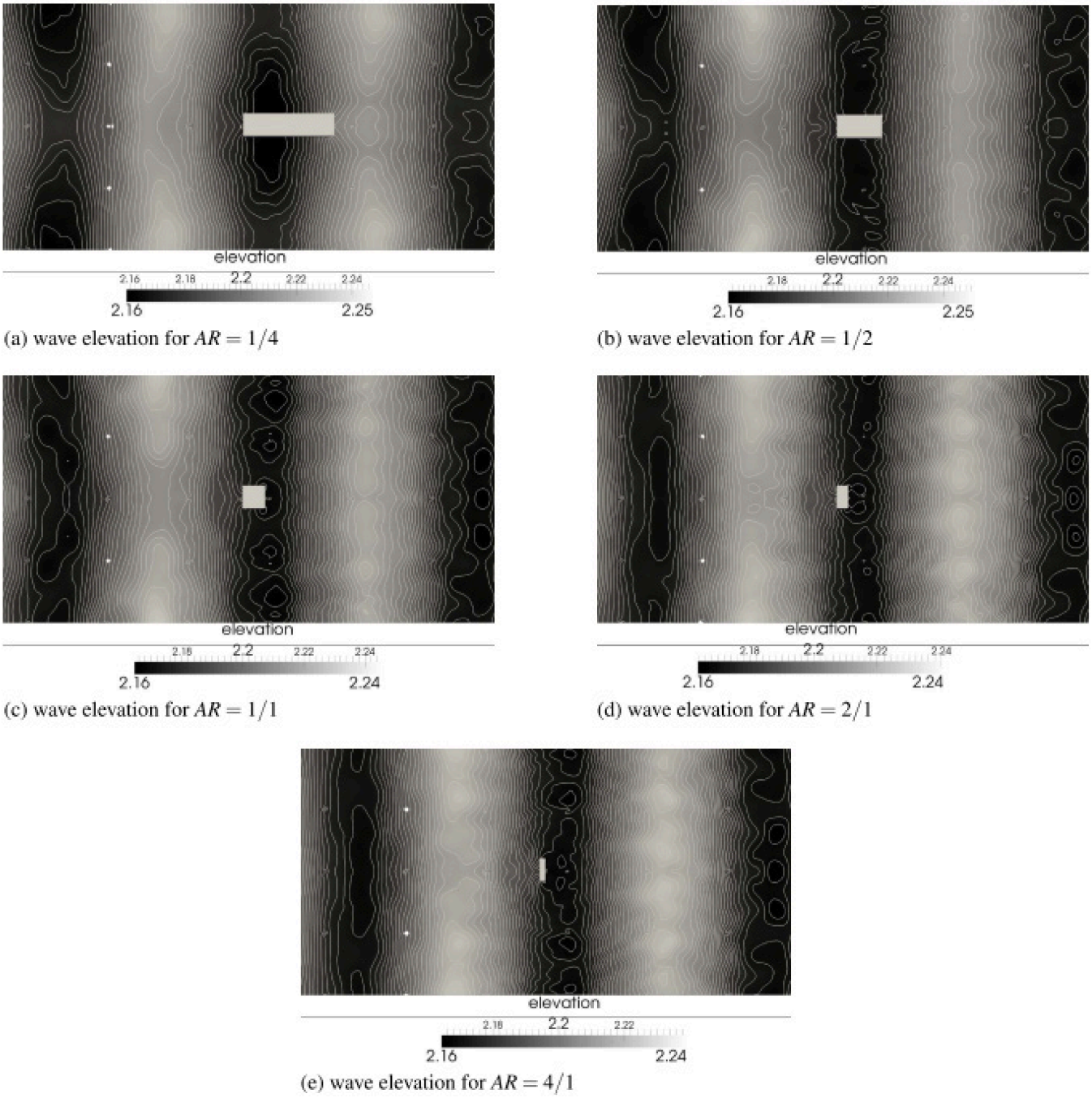

(a) wave elevation for $AR = 1/4$

(b) wave elevation for $AR = 1/2$

(c) wave elevation for $AR = 1/1$

(d) wave elevation for $AR = 2/1$

(e) wave elevation for $AR = 4/1$

Figure 5. Part of the domain showing wave elevation contours in the vicinity of the cylinder for various aspect ratios (AR) at t = 27.0s.

The free surface features around the cylinders is studied to obtain insight into the interaction of the flow with the rectangular cylinders of different aspect ratios in Figure 5. The wave elevation contours around the cylinder with the lowest aspect ratio of AR = 1/4 (Figure 5a) show a large difference in the water elevations in front and behind the cylinder. In this case, the dimension of the cylinder along the direction of wave propagation, l is of the order of half of the incident wavelength. This results in the presence of a trough behind the cylinder when a crest is incident in front of the cylinder. This large difference in water elevations results in the large wave forces acting on the cylinder. In Figure 5b, the aspect ratio is increased to AR = 1/2 and there is a reduction in the inline wave forces acting on the cylinder as the difference in the water elevations in front and behind is lower due to a shorter width l. The change in wave elevation contours in front and behind the cylinder is not as large as in Figure 5a for the previous case. The

front face of the cylinder in this case has the same water plane area as in the previous case (AR = 1/4) but a lower value of l results in a lower pressure difference between the front and the back faces, resulting in a lower inline force. On further increase in aspect ratio to AR = 1/1, the cross-section is now square-shaped. The inline wave forces on the cylinder show a large reduction from the values for AR = 1/4 and AR = 1/2. A change is observed in the pattern of the free surface elevation contours around the cylinder for AR = 1/1 in Figure 5c compared to the previous two cases with a lower aspect ratio. The low pressure region that is formed behind the cylinder in this case is smaller seen from the circular contours in place of the contours that terminate on the cylinder. The wave elevation contours in front and behind the cylinder have similar values implying a lower net pressure acting on the cylinder. This results in a considerably lower inline wave force in this case. In the next case, with AR = 2/1 (Figure 5d), the wave elevation contours show a pattern similar to that in the previous case with AR = 1/1 in Figure 5c. The inline wave force calculated in this case is slightly lesser than for AR = 1/1 as an increase in aspect ratio to AR = 2/1 results in a shorter width l and a lower net pressure on the cylinder. On increasing the aspect ratio to 4/1 in Figure 5e, the wave elevation contours are widely spaced behind the cylinder. The low width of the cylinder results in a similar wave phase in front and behind the cylinder and a low net pressure on the cylinder, which leads to a lower inline wave force on the cylinder in this case.

From the results above, it can be concluded that the aspect ratio of a rectangular cylinder influences the inline wave forces acting on the cylinder. The curve for the change in the force magnitude with a change in the width of the cross-section l with respect to the incident wavelength λ in Figure 6 is near-parabolic with the form:

$$\frac{l}{\lambda} = \left(\frac{F}{F_{sym}} \right)^2 \tag{3}$$

where F_{sym} is the inline wave force on a cylinder of aspect ratio 1/1. This implies that the increase in the inline wave force with an increase in the cross-sectional width l of the cylinder is large initially and then reduces with further increase in l/λ. This is justified by the fact that the major change in the inline force regime occurs when the width l of the cylinder is around the order of $\lambda/2$. In this range, the change in net pressure on the cylinder is large due to opposite phases (wave crest and trough) on the two sides of the cylinder.

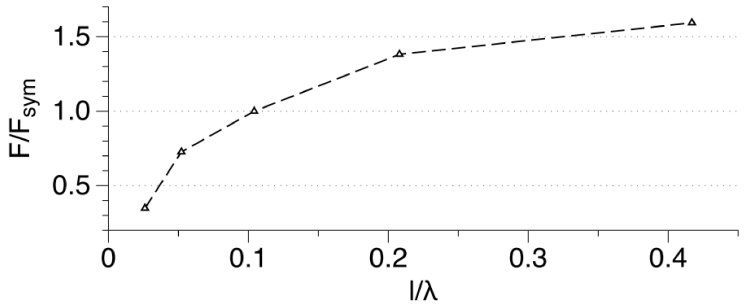

Figure 6. Variation of wave forces with the width l.

5 CONCLUSIONS

An open source CFD model was used to simulate wave interaction with truncated cylinders of rectangular cross-sections with different aspect ratios in a 3D numerical wave tank. The change in the inline wave forces acting on the cylinders for different aspect ratios is investigated. The wave elevation contours around the cylinders are studied to obtain a better understanding of the flow field around the cylinders. It is found that an increase in the aspect ratio results in a reduction of the wave forces acting on the cylinder. The phase of the force variation on a cylinder of smaller aspect ratio leads the force variation of that on a cylinder of a larger aspect ratio. The change in the magnitude of the inline wave force on the cylinder with increase in the ratio of the cylinder width along the direction of wave propagation to the wavelength is found to follow a near-parabolic trend.

6 ACKNOWLEDGEMENTS

This study has been carried out under the OWCBW project (No.217622/E20) and the authors are grateful to the grants provided by the Research Council of Norway. The study was supported in part by computational resources provided at the Norwegian University of Science and Technology by NOTUR, http://www.notur.no.

NOTATION

U	time-averaged velocity
ρ	density of the fluid
P	Pressure
v	viscosity of the fluid
v_t	eddy viscosity of the fluid
g	acceleration due to gravity
ϕ	level set function
k	turbulent kinetic energy
ω	specific turbulent dissipation rate
λ	wavelength
H	wave height
d	water depth
dx	grid size
b	dimension of the cylinder normal to the flow
l	dimension of the cylinder along the flow
AR	aspect ratio (b/l)
C_m	Morison added mass force coefficient
C_d	Morison drag force coefficient
F	Inline wave force
F_{sym}	Inline wave force on a cylinder of square cross-section (AR = 1/1)

REFERENCES

Bearman, P.W., Graham, J.M.R., Singh, S., 1979. Forces on cylinders in harmonically oscillating flow, in: Proc. Symp. on Mechanics of Wave Induced Forces on Cylinders, Bristol, (UK), pp. 437–449.

Durbin, P.A., 2009. Limiters and wall treatments in applied turbulence modeling. Fluid Dynamics Research 41, 1–18.

Egorov, Y., 2004. Validation of CFD codes with PTS-relevant test cases. Technical Report 5th Euratom Framework Programme ECORA project, EVOL-ECORA D07.

Jiang, G.S., Peng, D., 2000. Weighted eno schemes for Hamilton-Jacobi equations. SIAM Journal on Scientific Computing 21, 2126–2143.

Jiang, G.S., Shu, C.W., 1996. Efficient implementation of weighted ENO schemes. Journal of Computational Physics 126, 202–228.

Keulegan, G.H., Carpenter, L.H., 1958. Forces on cylinders and plates in an oscillating fluid. Journal of Research of the National Bureau of Standards 60, 423–440.

Larsen, J., Dancy, H., 1983. Open boundaries in short wave simulations - a new approach. Coastal Engineering 7, 285–297.

MacCamy, R., Fuchs, R., 1954. Wave forces on piles: A diffraction theory. University of California, Dept. of Engineering.

Mo, W., Irschik, K., Oumeraci, H., Liu, P., 2007. A 3D numerical model for computing non-breaking wave forces on slender piles. Journal of Engineering Mathematics 58, 19–30.

Morison, J.R., Johnson, J.W., O'Brien, M.P., 1954. Experimental studies of wave forces on piles, in: Proc., Fourth Coastal Engineering Conference.

Morison, J.R., O'Brien, M.P., Johnson, J.W., Schaaf, S.A., 1950. Force exerted by surface waves on piles. Journal of Petroleum Technology 2, 149–154.

Osher, S., Sethian, J.A., 1988. Fronts propagating with curvature- dependent speed: Algorithms based on hamilton-jacobi formulations. Journal of Computational Physics 79, 12–49

Peng, D., Merriman, B., Osher, S., Zhao, H., Kang, M., 1999. A PDE-based fast local level set method. Journal of Computational Physics 155, 410–438.

Sarpkaya, T., 1976. In-line and transverse forces on smooth and roughened cylinders in oscillatory flow at high Reynolds numbers, Report No. NPS-69SL76062. Naval Postgraduate School, Monterrey, California.

Vengatesan, V., Varyani, K.S., Barltrop, N., 2000. An experimental investigation of hydrodynamic coefficients for a vertical truncated rectangular cylinder due to regular and random waves. Ocean Engineering 27, 291–313.

Wilcox, D.C., 1994. Turbulence Modeling for CFD. DCW Industries Inc., La Canada, California.